# Numerical experiments on plasmoids entering a transverse magnetic field

H. Gunell,[1,a)] J. J. Walker,[1] M. E. Koepke,[1,b)] T. Hurtig,[2] N. Brenning,[3] and H. Nilsson[4]
[1]*Department of Physics, West Virginia University, Morgantown, West Virginia 26506-6315, USA*
[2]*Swedish Defence Research Agency, Grindsjön Research Centre, SE-147 25 Tumba, Sweden*
[3]*Division of Space and Plasma Physics, School of Electrical Engineering, Royal Institute of Technology,*
*SE-100 44 Stockholm, Sweden*
[4]*Swedish Institute of Space Physics, P.O. Box 812, SE-981 28 Kiruna, Sweden*

Plasma from the Earth's magnetosheath has previously been observed inside the magnetosphere. Inhomogeneities in the magnetosheath plasma, here called plasmoids, can impact the magnetopause and doing so set up a polarizing field that allows it to penetrate the magnetopause and enter the magnetosphere. A set of simulations of plasmoids with different dimensions is presented in this paper. For plasmoids that are longer than those previously published, waves propagating upstream from the barrier are found. It is also found that the penetration process causes the part of the plasmoid that is upstream of the barrier to rotate. The role of plasmoid width and cross sectional shape in penetration is studied, and for plasmoids that are less than half an ion gyroradius wide, the plasmoid is compressed to obtain a vertically oriented elliptical cross section, regardless of the initial shape. When the initial plasmoid width exceeds the ion gyroradius, the plasmoid still penetrates through a mechanism involving a potential that propagates upstream from the magnetic barrier. © 2009 American Institute of Physics. [doi:10.1063/1.3267860]

## I. INTRODUCTION

Plasma with characteristics of the shocked solar wind in the Earth's magnetosheath has, in the past, been measured on the inside of the magnetopause using rocket[1] and satellite[2,3] based instruments. Lemaire[4] suggested that inhomogeneities in the magnetosheath plasma could penetrate the magnetopause through a process called impulsive penetration. In this paper, such inhomogeneities are called plasmoids. In the laboratory, penetration of magnetic barriers have been observed in experiments with flowing plasmas.[5–8] Laser produced plasmas in magnetic fields have shown similar behavior.[9,10] It was shown experimentally that a background plasma can reduce the polarization field and prevent the plasmoid from penetrating the magnetic barrier if the background density is equal to or higher than the plasmoid density.[11] At the magnetopause, however, the density on the inside is lower than the density in the magnetosheath. Numerical studies of impulsive penetration, using both MHD and particle methods, were reviewed by Echim and Lemaire.[12] Early particle in cell simulations were performed by Koga *et al.*[13] covering a wide range of parameters. More recently, particle in cell simulations treating one case in more detail have been published.[14,15]

Brenning *et al.*[16] proposed that experiments and observations can be classified based on the kinetic beta

$$\beta_{\mathrm{k}} = W_K/W_B,$$

where $W_K = \frac{1}{2} n_0 m_i v_0^2$ is the kinetic energy density of the plasma and $W_B = B_\perp^2/(2\mu_0)$ its magnetic energy density, and on the penetrability parameter

$$\Pi = \frac{w}{r_{\mathrm{gi}}} K \sqrt{\beta_{\mathrm{ith}}},$$

where $w$ is the width of the plasmoid, $r_{\mathrm{gi}} = m_i v_0/(e B_\perp)$ the ion gyroradius, $\beta_{\mathrm{ith}} = \frac{1}{2} n_0 m_i v_{\mathrm{ith}}^2/W_B$ the ion thermal beta, and $K = 2.3$ is an empirically determined constant. Here $n_0$ is the plasma density, $m_i$ the ion mass, $\mathbf{v}_0$ the bulk velocity of the plasma, $B_\perp$ the component of $\mathbf{B}$ which is perpendicular to $\mathbf{v}_0$, and $v_{\mathrm{ith}}$ is the ion thermal speed. For $\beta_{\mathrm{k}} < 1$ a plasmoid is expected to penetrate through self-polarization if $\Pi < \sqrt{\beta_{\mathrm{k}}}$ and to be rejected for larger values of $\Pi$. For $\beta_{\mathrm{k}} > 1$ there is a third regime, where plasmoids can penetrate through expulsion if $\Pi > 1/\sqrt{\beta_{\mathrm{k}}}$, that is to say that for large $\beta_{\mathrm{k}}$-values the ambient magnetic field can be expelled by the plasmoid. A map of where experiments described in the literature can be found in $\beta_{\mathrm{k}}$-$\Pi$ space is shown in Fig. 8 of the paper by Brenning *et al.*[16] The parameters used in this paper can be found in Table I together with typical magnetopause parameters[17,18] and the experimental parameters of Hurtig *et al.*[14] The normalized plasmoid width $w/r_{\mathrm{gi}}$ and the penetrability parameter $\Pi$ are shown in Table II for the different simulation cases treated here. These simulations are all in the self-polarization regime.

In the self-polarization regime, when a plasmoid enters a transverse magnetic field, ions and electrons gyrate in opposite directions. Space charge sheaths will form on the edges of the plasmoid, and this will cause a polarization electric field $\mathbf{E} = -\mathbf{v} \times \mathbf{B}$ is set up inside that will enable the plasma to continue moving with its initial velocity by means of an $\mathbf{E} \times \mathbf{B}$-drift. The energy of the electric field is supplied by the kinetic energy of the plasma particles, and theory has predicted that the condition $W_K \gg W_E$ must be fulfilled for there to be enough energy to allow penetration.[19] Later it was shown that the requirement $W_K/W_E \gg \sqrt{m_i/m_e}$ is necessary to

---

a)Electronic mail: herbert.gunell@physics.org.
b)Also at: Division of Space and Plasma Physics, School of Electrical Engineering, Royal Institute of Technology, SE-100 44 Stockholm, Sweden.

TABLE I. Parameters at the magnetopause region (Refs. 17 and 18), the simulations presented here, and typical values for the experiments by Hurtig *et al.* (Ref. 14).

| Parameter | Simulation | Magnetopause[a] | Expt.[b] |
|---|---|---|---|
| $v_0/(km/s)$ | 300 | 100–200 | 300 |
| $n_0/m^{-3}$ | $10^{16}$ | $\approx 2 \times 10^7$ | $10^{18}$ |
| $B_\perp/T$ | 0.05 | $(10-30)\times 10^{-9}$ | 0.015 |
| $m_i/m_e$ | 92 | 1836 | 1836 |
| $\beta_k = W_K/W_B$ | $8 \times 10^{-4}$ | 0.5–17 | 0.8 |
| $W_K/W_E$ | 756 | $(0.4-4)\times 10^7$ | $8 \times 10^5$ |
| $\frac{1}{10}\frac{W_K}{W_E}\sqrt{\frac{m_e}{m_i}}$ | 7.9 | $(1-9)\times 10^4$ | $2 \times 10^3$ |

[a]References 17 and 18.
[b]Reference 14.

TABLE II. Normalized widths $w/r_{gi}$ penetrability parameters $\Pi = (w/r_{gi})K\sqrt{\beta_{ith}}$ and the center of the magnetic barrier $z_T$ for the different simulation cases presented here, and in the experiment (Ref. 14).

| | $w/r_{gi}$ | $\Pi$ | $z_T$ (cm) |
|---|---|---|---|
| Horizontal ellipse | 0.40 | $4.2 \times 10^{-3}$ | 16.5 |
| Circle | 0.40 | $4.2 \times 10^{-3}$ | 16.5 |
| Vertical ellipse | 0.13 | $1.4 \times 10^{-3}$ | 16.5 |
| Long plasmoid | 0.13 | $1.4 \times 10^{-3}$ | 31.5 |
| Wide plasmoid | 1.1 | $1.2 \times 10^{-2}$ | 16.5 |
| Expt.[a] | 0.5 | 0.1 | |

[a]Reference 14.

preserve quasineutrality.[20] Experimental studies showed that the requirement on the kinetic to electrostatic energy density ratio is $W_K/W_E > 10\sqrt{m_i/m_e}$ or else penetration is prevented.[6]

Experiments in the presence of a background plasma showed that the polarization electric field can be short-circuited by currents in this background plasma if its density is high enough.[11,21,22] A complete short circuit was obtained for a background density that was approximately 200 times higher than the plasmoid density. These measurements indicate that for background densities similar to the plasmoid density, plasmoid propagation should not be affected significantly by the background plasma. A plasmoid penetrating the dayside magnetopause from the magnetosheath will enter a region where the density is much lower. Therefore, no background density is included in the simulations presented here.

In a recent series of experiments waves in the lower hybrid frequency range were observed, and wave-driven electron transport perpendicular to both **B** and $v_0$ was seen.[7,8] The presence of waves in the lower hybrid frequency range has been seen in particle in cell simulations,[15] and *in situ* observations at the magnetopause by the Cluster spacecraft have also detected lower-hybrid waves.[17] In this paper we report numerical experiments that provide information on the penetration process. The simulation model is described in Sec. II. In Sec. III the influence of the cross sectional shape of the plasmoid on the outcome of penetration experiments is examined. In Sec. IV we report results of a simulation of a plasmoid that is longer than what has previously been simulated, and in Sec. V we explore the penetration mechanism for a plasmoid that is wider than $r_{gi}$.

## II. NUMERICAL APPROACH

We have used the three-dimensional electrostatic particle-in-cell code that was first used by Hurtig *et al.*[14] and later by Gunell *et al.*[15] The code uses open boundary conditions, which means that when the charge of the particles has been assigned to the grid the potential on the boundaries of the simulation box is calculated, assuming empty space between these boundaries and infinity. Poisson's equation is then solved using the potential thus obtained as a Dirichlet

boundary condition. The simulation grid moves with the initial velocity of the plasmoids, making the computations more efficient by allowing us to solve Poisson's equation only in the region near the plasma cylinder and not in the empty space in front of and behind it.

A schematic of the simulation geometry is shown in Fig. 1 The example shown in Fig. 1 is the initial geometry of the simulation case that is presented in Sec. IV. In all cases the initial bulk velocity of the plasmoid is $v_0 = 300$ km/s in the z-direction. The magnetic field is

$$\mathbf{B} = \mathbf{B}_0\left[\left(\frac{1}{1 + e^{(z-z_T)/\delta}} - 1\right)\hat{\mathbf{y}} + \hat{\mathbf{z}}\right],$$

where $\mathbf{B}_0$ is the horizontal component of the magnetic field, $\delta = 20$ mm is a characteristic length related to the length of the transition, and $z_T$, which is tabulated in Table II, is the z-coordinate of the center of the transition region.

A few words should be said about the applicability of these simulations. The requirements on computer simulations are quite different for different parts of $\beta_k$-$\Pi$ space. In the expulsion regime, mentioned in Sec. I, the magnetic field is deformed since it cannot penetrate the plasmoid, and that process would require electromagnetic simulations for it to be modeled correctly. For the simulations presented here, $\beta_k = 8 \times 10^{-4} \ll 1$. Thus, the electrostatic approximation is valid and there is no magnetic field deformation. The question that arises is, what is the upper limit in $\beta_k$ for which these, low $\beta_k$, simulations still can teach us something about what happens in the plasma? Hurtig *et al.*[8] conducted experiments with $\beta_k$ in a range from 0.1 to 10, and found that the plasmoids penetrate through self-polarization for $\beta_k \lesssim 3$. Since the present and the previous[15] simulations also reproduce wave phenomena seen in these experiments, they should at least be able to tell us something about the lower half of that $\beta_k$ range. Wessel *et al.*[11] reported experiments where the relative magnetic field change $\Delta B/B_0$ was much less than unity even for $\beta_k = 400$. In cases where there is resistivity, for example, provided by wave activity, the magnetic field can enter the plasmoid without appreciable deformation, and electrostatic phenomena can be dominating even for high values of $\beta_k$.
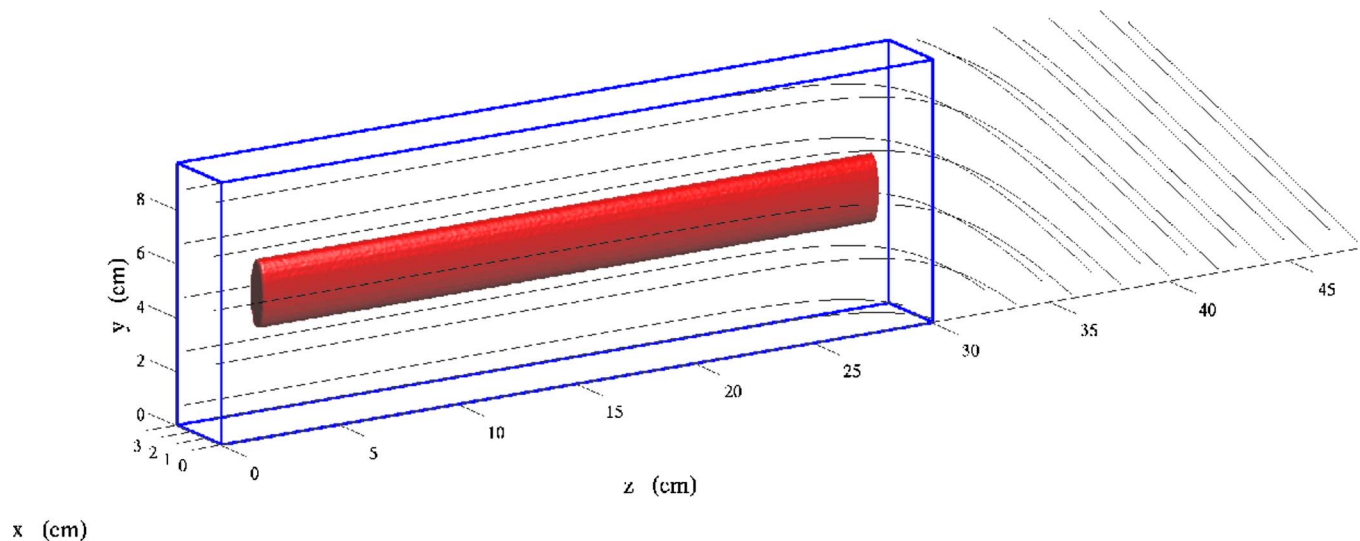
FIG. 1. (Color online) Initial simulation geometry for the long plasmoid presented in Sec. IV.

## III. CROSS SECTIONAL SHAPES

It has been observed in laboratory experiments that the plasmoid is compressed perpendicularly both to its velocity and the magnetic field.[5,14] This compression is caused by the $\mathbf{j} \times \mathbf{B}$-force arising from the diamagnetic current,[14] and it has also been seen in simulations.[15] A similar compression has also been observed in laser produced plasmas.[10] We performed a numerical experiment to determine the influence of the initial cross sectional shape of the plasmoid. We compare the circular cross section that was studied previously[15] with two elliptical cross sections: one oriented horizontally and one vertically. The three different cross sections are drawn in Fig. 2. The widths of these three are all less than $r_{gi}/2$. The larger ellipse shows the cross section of the wide plasmoid, which is described in Sec. V.

Figure 3 shows cross sections in the $xy$-plane through the center $z$-coordinate for the three different plasmoids for times $t=0.4$, 200, and 400 ns. The horizontally elliptic cross section is shown in the left column; the circular cross section in the central column; and the vertically elliptic cross section is shown in the right column.

In all three cases the plasmoid is compressed as it moves into the transverse field region, and after 400 ns the cross section has become a vertically extended structure regardless of its initial shape. The initial density is $1.0 \times 10^{16}$ m$^{-3}$ in all the three cases. The total plasma content is larger in the case of the plasmoid with the circular cross section and as it is compressed this leads to the larger densities that are seen at later simulation times. In the two elliptical cases, the cross sectional area remains approximately constant during compression, and therefore the density remains at about $1.0 \times 10^{16}$ m$^{-3}$. The extremities that extend from the main body of the plasma in all cases at $t=400$ ns are a sign of the development of waves in the lower hybrid frequency range as the plasmoid enters the transverse field region.

## IV. LONG PLASMOIDS

We performed one simulation run of the 26 cm long plasmoid that is shown in Fig. 1. This is more than twice the length of the previously published plasmoid,[15] which was 11 cm. For the initial cross sectional shape the vertical ellipse of Sec. III was chosen. Since all shapes are compressed to a vertical ellipse, and the different cases otherwise exhibit the same behavior, this should be equivalent to using a circular cross section. With this choice of plasmoid shape, the simulation box can be chosen to be narrower in the $x$-direction, thus avoiding unnecessary empty space and using the computational resources more efficiently.

Figure 4 shows the plasma density of the long plasmoid simulation in the $xy$-plane (left column) and the $yz$-plane (right column) for the times $t=80$, 360, 640, and 920 ns from
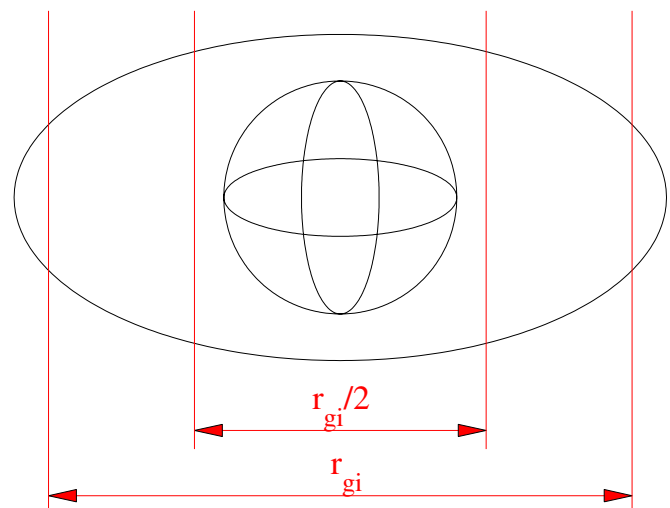


FIG. 2. (Color online) The different initial cross sectional shapes of the plasmoid simulations presented in this article.
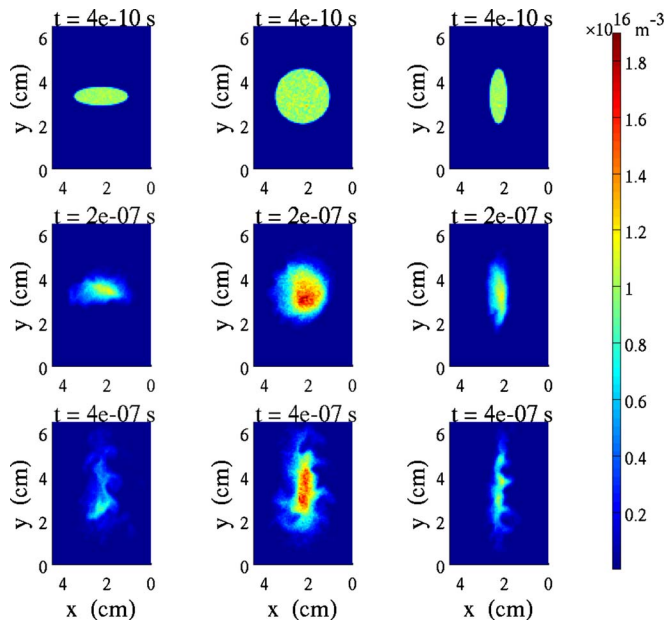
FIG. 3. (Color online) The development of the cross section for three different initial shapes. The left column shows the horizontal ellipse; the middle column shows the circular cross section; and the right column the vertical ellipse. The top row shows a cross section of the density after one time step. The middle and bottom rows show the same cross section after the simulations have run for 500 and 1000 time steps, respectively.

top to bottom. Field aligned wave structures develop as the plasmoid enters the transverse field region. At $t=360$ ns, shown in the second row of Fig. 4, only one third of the plasmoid has entered the transverse field region. However, field aligned structures are seen all along the plasmoid, i.e., also in the upstream horizontal field region. Thus, there is a wave that propagates in the direction opposite to the plasmoid velocity. The upstream structures that are seen in the $yz$-plane are not detached from the main body of the plasmoid, but, as can be seen from the slice in the $xy$-plane, they are rather a result of a nonrigid rotation of the plasmoid. At later times (bottom row of Fig. 4) the plasmoid moves toward lower $x$-values, and moves out or the slice that is shown in the $yz$-plane. This motion is more clearly seen in the $xz$-plane, which is shown in Fig. 5. The motion in the negative $x$-direction is consistent with the beginning of a cycloid trajectory for an ion moving in electric and magnetic fields if $E/B_\perp > v_0$, which is true inside the plasmoid in the transverse field region. This is also consistent with experimental observations[9] and theory.[23]

The upper panel of Fig. 6 shows the density as it would be measured by a probe located at $(x,y,z) = (17.5, 48.75, 390)$ mm. The $x$-coordinate of the probe is shifted 2.5 mm from the center of the plasma $(x_0 = 15.0$ mm) toward the high potential side. The lower
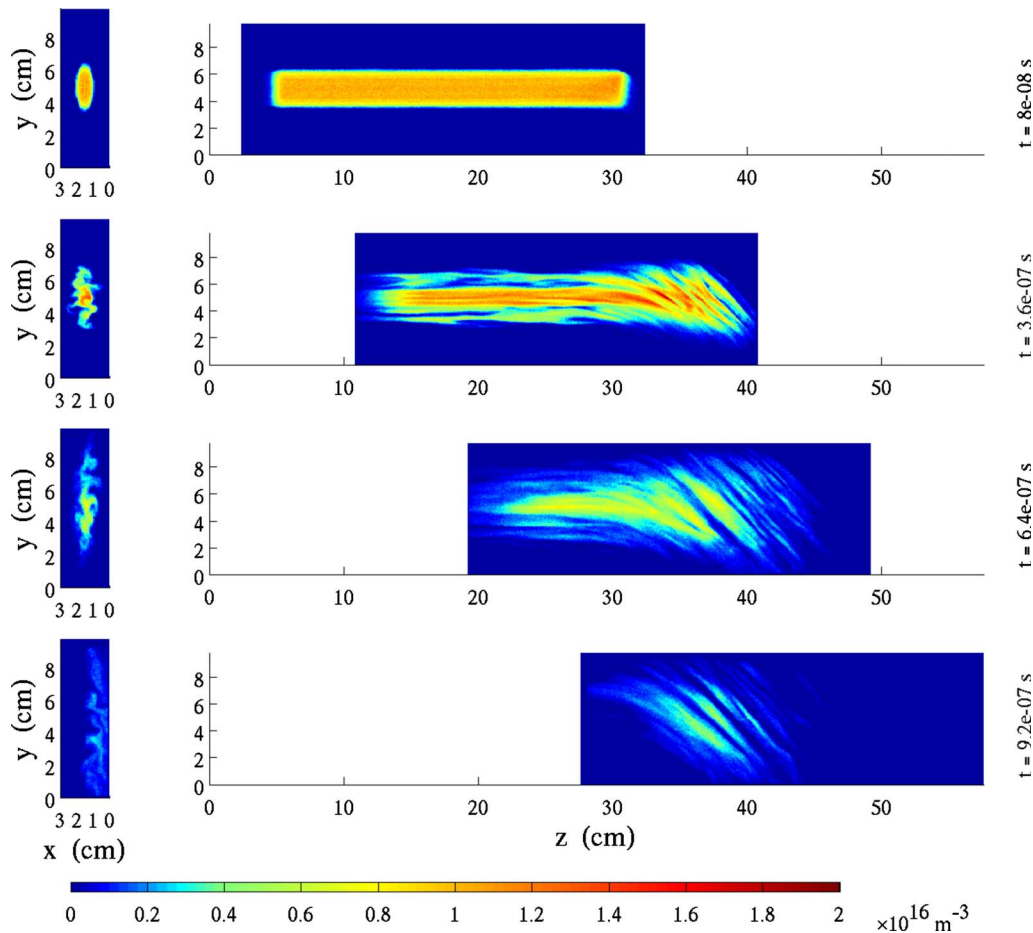


FIG. 4. (Color online) Slices of the electron density of the long plasmoid simulation in the $xy$-plane (left column) and the $yz$-plane (right column) for times $t = 80, 360, 640,$ and $920$ ns.
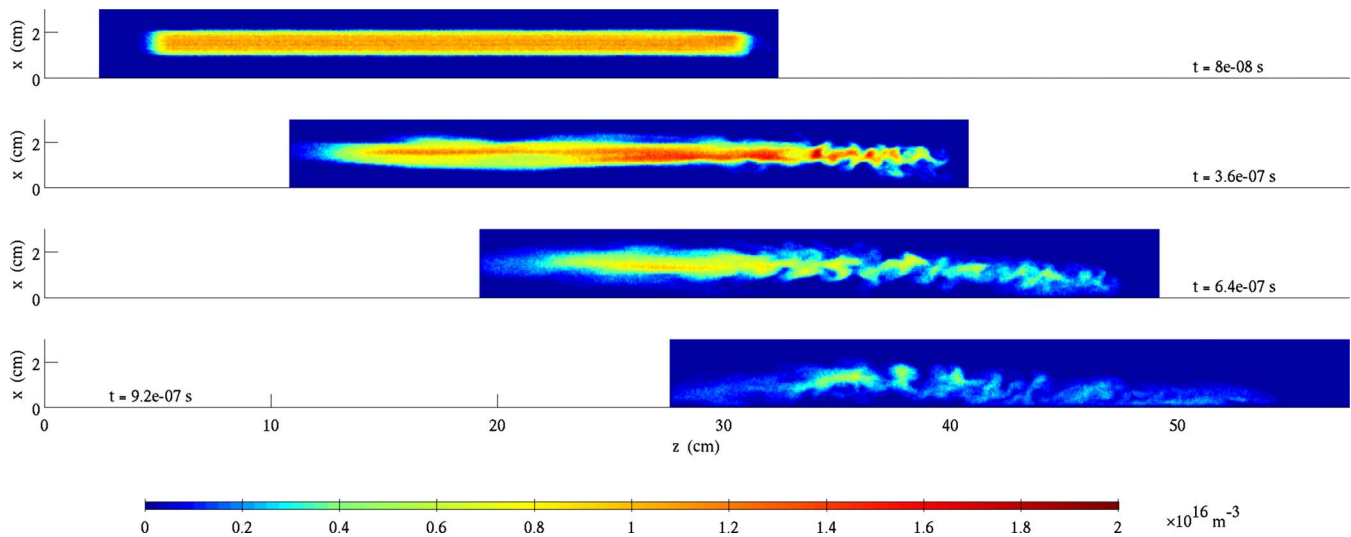
FIG. 5. (Color online) Density in the $xz$-plane of the long plasmoid for times $t=80$, 360, 640, and 920 ns.

panel shows the power spectral density $P_{nn}$ of $n_p - \langle n_p \rangle$, where $n_p$ is the density measured by the probe and $\langle n_p \rangle$ is the mean value of the density during the time shown in the upper panel.

## V. WIDE PLASMOIDS

It was suggested by Lindberg[5] that plasmoids wider than half the ion gyroradius cannot penetrate unless they break up into smaller plasmoids. While Lindberg's limit was derived under simplifying assumptions that may not always be applicable, it is still interesting to study the transition from narrow plasmoids, with $w \ll r_{gi}$, to wide plasmoids, where $w \gg r_{gi}$. Experiments[9] have shown that wide plasmoids can break up into narrower plasmoids, and theory[23] suggests that the Rayleigh–Taylor instability is a possible mechanism for this.

The wide plasmoid limit is computationally more demanding, and it will be in studied in the future. The behavior of plasmoids in the transition region ($w \approx r_{gi}$) can be investigated more easily. We have simulated a plasmoid with a width $w=1.1r_{gi}$. The initial cross section is shown by the largest ellipse in Fig. 2. Figure 7 shows the plasma density in the simulation of the wide plasmoid in the $xy$-plane (left column) and the $yz$-plane (right column) for the times $t=40$, 240, 440, and 640 ns from top to bottom. Figure 8 shows a slice of the density in the $xz$-plane for times $t=40$, 240, 440, and 640 ns. Wave structures similar to those in the long plasmoid case, shown in Fig. 4, are also seen in for the wide plasmoid in Fig. 7. The amplitude is not as large in Fig. 7 as in the narrower plasmoid shown in Fig. 4. The density in the $yz$-plane that is shown in the right column of Fig. 7 is a slice through the central $x$-coordinate of the plasmoid ($x=4.5$ cm), where the current density is smaller than along the plasmoid edges. That the wave amplitude is higher along the plasmoid sides can be seen in the density slice in the $xy$-plane for $t=440$ ns and also in the $xz$-plane shown in the corresponding panel of Fig. 8. The current flows around the plasmoid in the $xz$-plane. This current gives rise to waves along the front of the plasmoid, as can be seen in the second

panel of Fig. 8. For the narrower plasmoids of Secs. III and IV, this effect is not seen since the width does not allow more than one wavelength in the $x$-direction.

The plasmoid does not break up into smaller plasmoids. At later simulation times, in the lower panels of Fig. 8 a compression of the plasmoid in the $x$-direction can be seen. We also observe that, while the plasmoid was deformed sig-
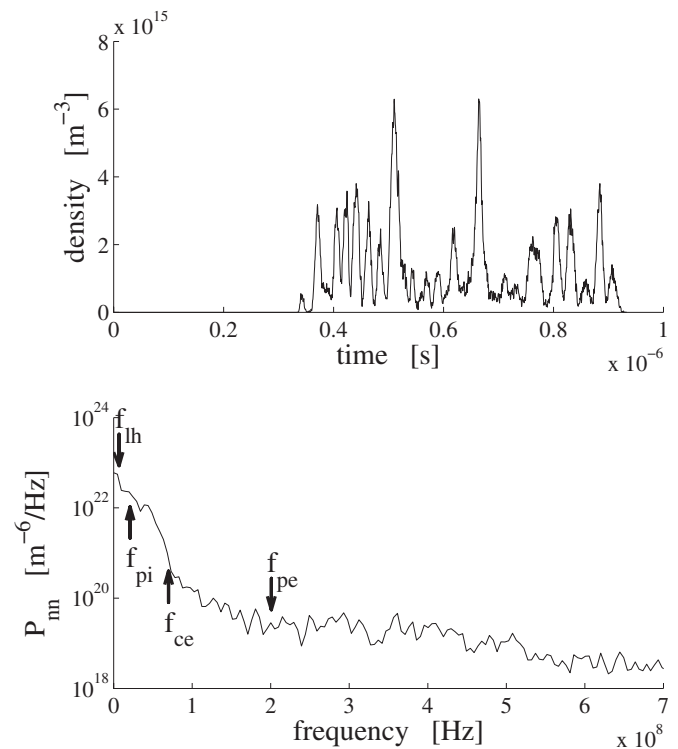


FIG. 6. The upper panel shows the signal from a density-measuring virtual probe located at $x=17.5$ mm, $y=48.75$ mm, $z=390$ mm in simulation of the long plasmoid. The lower panel shows the power spectral density of this signal after subtraction of its mean value. The lower-hybrid frequency, the ion and electron plasma frequencies, and electron cyclotron frequency are marked using arrows in the lower panel.
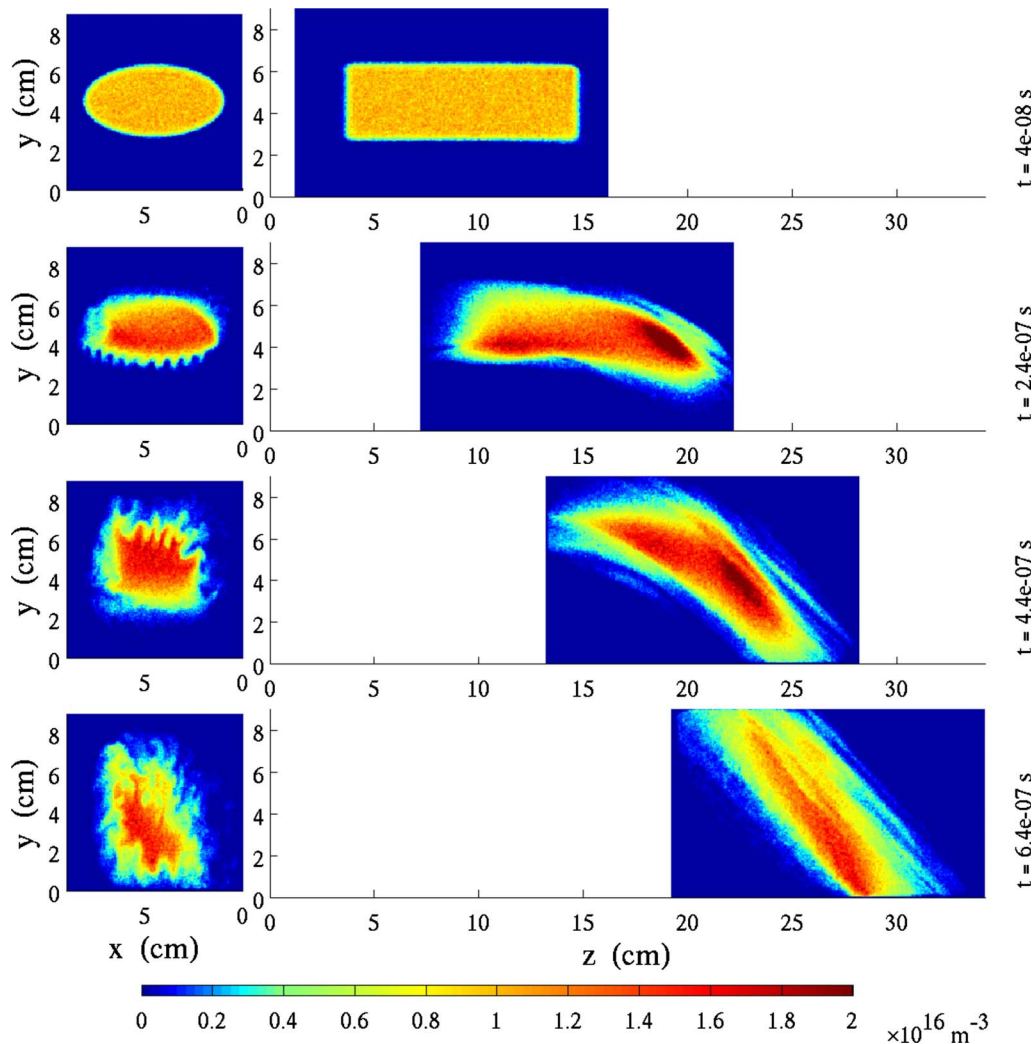
FIG. 7. (Color online) Slices of the electron density of the wide plasmoid simulation in the *xy*-plane (left column) and the *yz*-plane (right column) for times $t=40$, 240, 440, and 640 ns.

nificantly when it entered the transverse field region, it did penetrate the barrier.

Figure 9 shows the potential in the *xz*-plane at $y=4.5$ cm in the simulation of the wide plasmoid for times $t=40$, 240, 440, and 640 ns. The black line in Fig. 9 shows where the density is $5 \times 10^{15}$ m$^{-3}$, i.e., half the initial density. The magnetic field lines in the *yz*-plane for the same simulation times are shown in Fig. 10. As soon as the plasmoid starts entering the transverse field region, a positive potential propagates upstream at higher *x*-values outside the plasmoid itself. This is seen already at $t=40$ ns (top panel of Fig. 9) when only the front of the plasmoid is experiencing a modest transverse field component (see Fig. 10). In the next panel, i.e., at $t=240$ ns, the positive potential has propagated all the way to the back of the plasmoid. This upstream propagating potential sets up the polarization field that enables the particles to $\mathbf{E} \times \mathbf{B}$-drift with approximately their initial velocity. Since the potential propagates upstream at the plasmoid edge, only very few ions at the edge will experience an electric field *z*-component that would slow them down. The vast majority of the plasmoid particles will experience only the *x*-component polarization electric field that enables their penetration.

## VI. SUMMARY AND DISCUSSION

We have performed a series of numerical experiments to study the impulsive penetration process. When a plasmoid enters a transverse field region, a diamagnetic current is set up. This current acts to compress the plasmoid sideways, i.e., in a direction that is orthogonal to both the magnetic field and the plasmoid velocity, via a $\mathbf{j} \times \mathbf{B}$-force. For narrow plasmoids, the widths of which are less than $r_{\mathrm{gi}}/2$ this means that the initial cross sectional shape of the plasmoid does not influence the outcome of the experiment. Regardless of its initial shape, when the plasmoid enters the transverse field, it is compressed into an oblong structure, which is aligned with the transverse magnetic field. Once they have passed into the transverse field, the initially different plasmoids exhibit all the same wave phenomena as the previously published plasmoid with a circular cross section.[15]
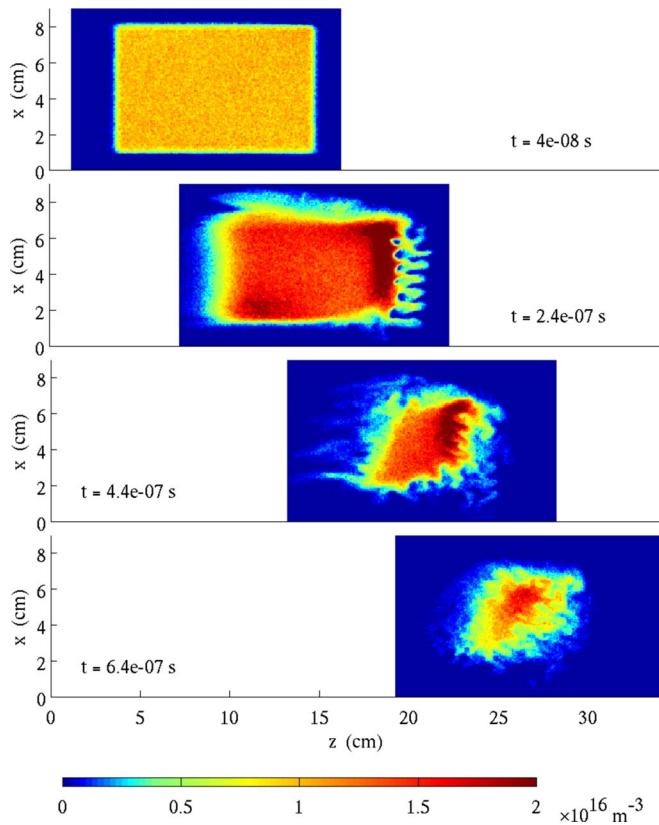
FIG. 8. (Color online) Density in the $xz$-plane of the wide plasmoid for times $t=40$, 240, 440, and 640 ns.

In simulations of a plasmoid which is longer than in previous simulations, it is found that a wave travels from the magnetic barrier in the direction opposite to the plasmoid velocity, and that this causes a nonrigid rotation of the upstream plasmoid. Structures such as those in the second row of Fig. 4 should be possible to detect in the magnetosheath of the Earth for plasmoids that are in contact with the magnetopause, and this would be a way to distinguish these from plasmoids that are not. It is also seen that the plasmoid moves perpendicularly in the direction of the electron rotation, in agreement with theory[23] and experiments in laser produced plasmas,[9] but in the direction opposite to that of the wave-driven transport that has been observed in plasma gun experiments.[7,8]

The penetration mechanism for plasmoids that are wide compared to the ion gyroradius is of particular interest in magnetopause physics. Spatial structures in the magnetosheath, that is to say, plasmoids are expected to be large on the order of the radius of the Earth, $(0.1R_E - 10R_E$ as seen in Cluster data[24]), whereas the plasmoids that can penetrate through self-polarization are on the order of 10–100 km according to a simple estimate.[15] In experiments with laser produced plasmas, wide plasmoids have been seen to break up into smaller plasmoids that convect across magnetic field lines. It has been suggested that plasmoids can break up under a Rayleigh–Taylor instability, and this is in agreement with theory.[23] In this paper we have presented a simulation of a plasmoid that is $1.1r_{gi}$ wide. The fingerlike structure that develops at the front of the plasmoid as it enters the trans-
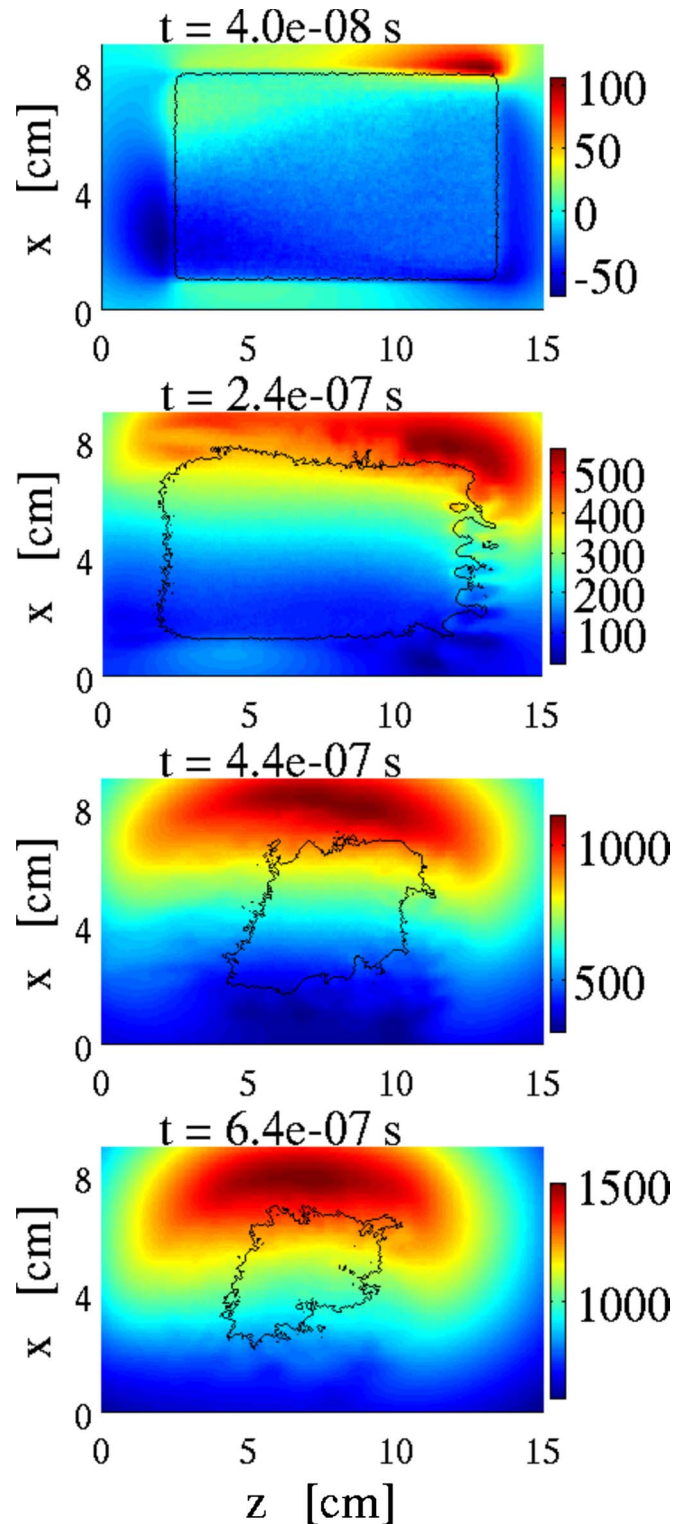


FIG. 9. (Color online) Potential (color-coded) in the $xz$-plane in the simulation of the wide plasmoid for times $t=40$, 240, 440, and 640 ns. The curve that is overlaid on the image shows where the density is $5 \times 10^{15}$ m$^{-3}$, i.e., half the initial density. In all cases the potential is shown for $y=4.5$ cm.

verse field region has the same wavelength as the waves in the lower hybrid frequency range that travel along the plasmoid direction of motion. The diamagnetic current that is set up when the plasmoid enters the transverse field flows in the $x$-direction, across the front of the plasmoid, and the relative
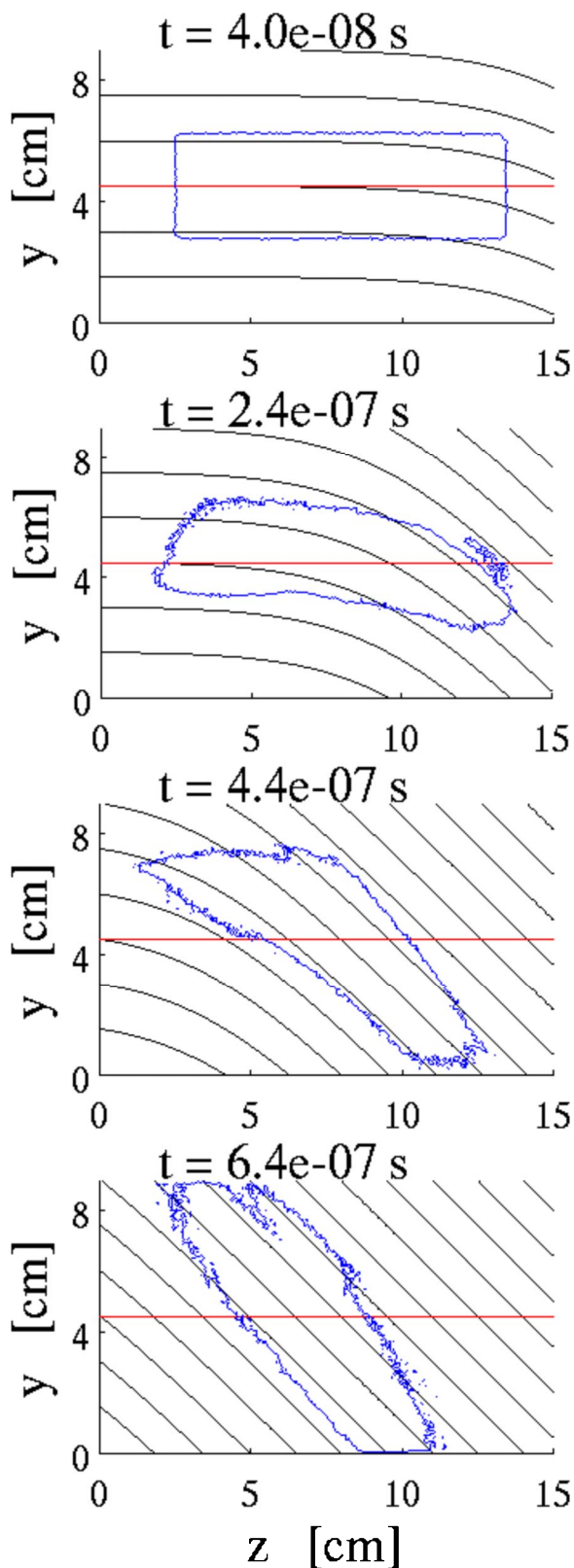
FIG. 10. (Color online) Magnetic field lines and density contour in the *yz*-plane in the simulation of the wide plasmoid for times *t*=40, 240, 440, and 640 ns. The irregularly shaped curve shows where the density is 5 $\times 10^{15}$ m$^{-3}$, i.e., half the initial density. The horizontal straight line shows the *y*-coordinate for which the potentials are shown in Fig. 9.

drift between electrons and ions creates the waves through a two-stream instability. This is therefore not a sign of a Rayleigh–Taylor mechanism. The fingers also disappear later in the simulation. In the simulated case, the polarization electric field travels back from the magnetic barrier to the upstream part of the plasmoid. Ions are thereby elevated to a higher potential without being slowed down by a longitudinal electric field. The plasmoid is also compressed in the cross field direction during the penetration.

Future research should include simulations of even wider plasmoids, so that it can be determined whether the rejection regime is encountered first as we move to larger $\Pi$-values or whether it breaks up under the Rayleigh–Taylor instability. It is also of interest to study the sideways compression and the backward propagating potential for wider plasmoids.

## ACKNOWLEDGMENTS

[1] C. W. Carlson and R. B. Torbert, J. Geophys. Res. **85**, 2903, doi:10.1029/JA085iA06p02903 (1980).
[2] J. Woch and R. Lundin, J. Geophys. Res. **97**, 1431, doi:10.1029/91JA02490 (1992).
[3] R. Lundin, J.-A. Sauvaud, H. Rème, A. Balogh, I. Dandouras, J. M. Bosqued, C. Carlson, G. K. Parks, E. Möbius, L. M. Kistler, B. Klecker, E. Amata, V. Formisano, M. Dunlop, L. Eliasson, A. Korth, B. Lavraud, amd M. McCarthy, Ann. Geophys. **21**, 457 (2003).
[4] J. Lemaire, Planet. Space Sci. **25**, 887 (1977).
[5] L. Lindberg, Astrophys. Space Sci. **55**, 203 (1978).
[6] H. Ishizuka and S. Robertson, Phys. Fluids **25**, 2353 (1982).
[7] T. Hurtig, N. Brenning, and M. A. Raadu, Phys. Plasmas **11**, L33 (2004).
[8] T. Hurtig, N. Brenning, and M. A. Raadu, Phys. Plasmas **12**, 012308 (2005).
[9] B. H. Ripin, E. A. McLean, C. K. Manka, C. Pawley, J. A. Stamper, T. A. Peyser, A. N. Mostovych, J. Grun, and J. Huba, Phys. Rev. Lett. **59**, 2299 (1987).
[10] A. N. Mostovych, B. H. Ripin, and J. A. Stamper, Phys. Rev. Lett. **62**, 2837 (1989).
[11] F. J. Wessel, R. Hong, J. Song, A. Fisher, N. Rostoker, A. Ron, R. Li, and R. Y. Fan, Phys. Fluids **31**, 3778 (1988).
[12] M. M. Echim and J. F. Lemaire, Space Sci. Rev. **92**, 565 (2000).
[13] J. Koga, J. L. Geary, T. Fujinami, B. S. Newberger, T. Tajima, and N. Rostoker, J. Plasma Phys. **42**, 91 (1989).
[14] T. Hurtig, N. Brenning, and M. A. Raadu, Phys. Plasmas **10**, 4291 (2003).
[15] H. Gunell, T. Hurtig, H. Nilsson, M. Koepke, and N. Brenning, Plasma Phys. Contr. Fusion **50**, 074013 (2008).
[16] N. Brenning, T. Hurtig, and M. A. Raadu, Phys. Plasmas **12**, 012309 (2005).
[17] M. André, R. Behlke, J.-E. Wahlund, A. Vaivads, A.-I. Eriksson, A. Tjulin, T. D. Carozzi, C. Cully, G. Gustafsson, D. Sundkvist, Y. Khotyaintsev, N. Cornilleau-Wehrlin, L. Rezeau, M. Maksimovic, E. Lucek, A. Balogh, M. Dunlop, P.-A. Lindqvist, F. Mozer, A. Pedersen, and A. Fazakerley, Ann. Geophys. **19**, 1471 (2001).
[18] D. Sundkvist, A. Retinò, A. Vaivads, and S. D. Bale, Phys. Rev. Lett. **99**, 025004 (2007).
[19] G. Schmidt, Phys. Fluids **3**, 961 (1960).
[20] W. Peter and N. Rostoker, Phys. Fluids **25**, 730 (1982).
[21] R. Hong, F. J. Wessel, J. Song, A. Fisher, and N. Rostoker, J. Appl. Phys. **64**, 73 (1988).
[22] F. J. Wessel, N. Rostoker, A. Fisher, H. U. Rahman, and J. H. Song, Phys. Fluids B **2**, 1467 (1990).
[23] A. B. Hassam and J. D. Huba, Geophys. Res. Lett. **14**, 60, doi:10.1029/GL014i001p00060 (1987).
[24] T. Karlsson, private communication (2009).